

**INVESTIGATION OF
STRUCTURE-PROPERTY CORRELATION IN
INTERMETALLIC COMPOUNDS**

PRABUDDHA KANT MISHRA



DEPARTMENT OF CHEMISTRY

INDIAN INSTITUTE OF TECHNOLOGY DELHI

August 2024

© Indian Institute of Technology Delhi (IITD), New Delhi, 2024

**INVESTIGATION OF
STRUCTURE-PROPERTY CORRELATION IN
INTERMETALLIC COMPOUNDS**

by

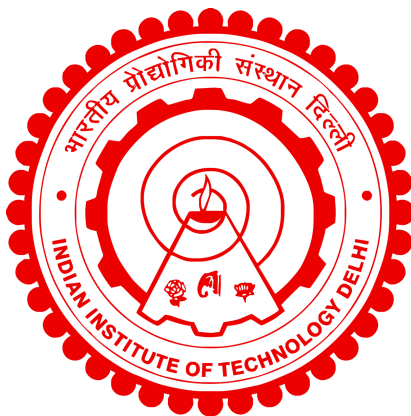
Prabuddha Kant Mishra

Department of Chemistry

Submitted

in fulfillment of the requirements of the degree of Doctor of Philosophy

to the



INDIAN INSTITUTE OF TECHNOLOGY DELHI

August 2024

Dedicated to

the great Music composer and Gazal singer... Jagjit Singh

Certificate

This is to certify that the thesis entitled “**Investigation of structure-property correlation in Intermetallic compounds**”, submitted by **Mr. Prabuddha Kant Mishra** to the Indian Institute of Technology Delhi, for the award of the degree of **Doctor of Philosophy** in Chemistry, is a record of the original, bona fide research work carried out by him under our supervision and guidance. The thesis has reached the standards fulfilling the requirements of the regulations related to the award of the degree.

The results contained in this thesis have not been submitted in part or in full to any other University or Institute for the award of any degree or diploma to the best of our knowledge.



Prof. Ashok K. Ganguli
Department of Chemistry,
Indian Institute of Technology Delhi
New Delhi-110016
INDIA

Prof. Pramit K. Chowdhury
Department of Chemistry,
Indian Institute of Technology Delhi
New Delhi- 110016
INDIA

Acknowledgements

This thesis is the culmination of a five-year-long endeavour, characterised by extensive collaboration and teamwork, in which a multitude of individuals have made unwavering contributions, both directly and indirectly. At this moment of recognition, I may inadvertently overlooked a few individuals and would like to apologise for that.

I would like to start by conveying my appreciation to my thesis mentor, Prof. Ashok K. Ganguli, for giving me the chance to work in the captivating domain of inter-metallic compounds, a subject of research interest for decades and has recently gained prominence in spintronics. During my PhD journey, I have found his continuous support and research guidance in our IIT-lab and other collaborations. Due to his constant support and belief in my abilities, I was able to synthesize and explore the physical properties of different classes of compounds. Our lab always has benefited from positive and continuous efforts in academia. I feel gratitude for his efforts to make our lab prosperous, this has made our work more focused. I am truly blessed to have a supervisor with efficient and dynamic personality, whose guidance serves as a source of inspiration for all of us. However, my utmost admiration is due to his availability for research discussions and 100 % support.

Now, I would like to express my gratitude to my collaborators, Prof. Ratanmala Chatterjee, who have always been very kind to me and supported me in various research activities including the GIMRT program. I am fortunate to have academic support from Japan through Prof. Rie Umetsu, her energy and positivity have inspired me a lot. Her mentorship has allowed me to gain a diverse, multidisciplinary education and the chance to collaborate with some exceptional individuals. In the fourth year of my PhD, I had the privilege to work with Prof. B. K Mani .His clarity about concepts and urge to convey it more profoundly in articles has motivated me and sharpened my articulacy. Apart from his theoretical investigations in the manuscript, I admire him for his kind nature and willingness to discussions to make us understand the subject better. I would like to extend my gratitude to Prof. Niharika Mohapatra from IIT Bhubaneswar, who has always been involved as a backing hand to support by research activities and shaping the manuscripts. With the invaluable contributions of all above mentioned people in both experimental and

theoretical aspects of various projects, the thesis has got its current shape. I am grateful for their enthusiasm in assisting me for comprehending the crucial elements in resolving any uncertainties.

I would like to express my gratitude to my research committee members for their valuable comments and suggestions, which have greatly enriched my thesis. I would also like to express my thanks to all the past and present Head of the Department of Chemistry at IIT Delhi for their support in providing the necessary facilities required for the completion of my thesis. Additionally, I am grateful to all the faculty and staff members of the Department of Chemistry, for their assistance and support throughout my academic journey. I want to acknowledge the Central Research Facility (CRF) and the Nano Research Facility (NRF) at IIT Delhi for providing access to facilities necessary for the completion of my research. Additionally, I would like to thank CSIR and GIMRT for the financial support, enabling me to pursue my academic aspirations and contribute to the advancement of knowledge in my field.

I am fortunate to be part of SSNRL at IIT Delhi where I met several good lifelong friends. Their good experimental skills are surplus and I have always benefited from them. However, I never felt seeking emotional support, still their presence have made me happy and involved. I am sure that we will be always in touch with each other and that's why at this time of submission of PhD, I have no feeling of grief due to this physical separation. With Brahma and Aarti, as a team, I became more productive with enhanced capabilities. They are source of power and courage to me. Although I don't share the research area with Manisha and Akshita, we have a natural connection, which is precious to me.

My sincere thanks go to the Solid State and Nanomaterial Research Lab, especially Lab 235 and 227, where I conducted my Ph.D. research. The time spent there was invaluable for my academic and personal growth, and I cherish the vibrant, intellectually stimulating environment of Lab. I am deeply thankful to the members of my research group, both past and present. I would like to particularly acknowledge Dr. Nitin Yadav, Dr. Sandeep Kumar, Dr. Vaishali, Dr. Preeti Dagar, Dr. Shalini Tiwari, Dr. Moumita Naskar, Dr. Anirban Das, Dr. Antara, Dr. Soumen Ash, Dr. Priyanka Yadav, Dr. Kirandeep, Manisha, Akshita, Manoj, Nitika, Ipshita, Aarti, Haribrahma, and Archita for their support and encouragement. Special thanks to Dr. Sandeep Dhaka for being not only a mentor but also a dear friend, always

ready with advice and encouragement. Most of time of my PhD, I was close to current and junior colleagues Manisha, Akshita, Nitika, Ipshita, Aarti, Haribrahma, Archita, and Sanjeev. They all are very dear to me.

I am equally grateful to my friends from physics department, IIT Delhi (Gaurav, Divya, Balwant, Vikas, Mohan, Anupam, Majhi and Deepak) collaborators at IIT Bhubaneswar (Soumya Kant Panda), at IISc (Darshit) and at JNCSR (Souvik) for their support.

I would like to express my heartfelt appreciation to my close friend Shreyash, Vinod, Peeus, Pandey, Rahul, Aanand, Sandeep Tripathi, Anjali, Jaydeep, Shubham, Kishan, Himanshu, for their unwavering and unconditional support, both emotionally and financially, throughout this journey. On a personal note, I would like to thank my family and friends for their limitless support and understanding. To my parents, thank you for your endless love, encouragement, and belief in my capabilities. To my siblings, your support has been a constant source of strength. To my unmentioned friends, thank you for your patience and for being my anchors through this demanding journey. To all those who have supported, encouraged, and contributed to this journey whether through words of encouragement, acts of kindness, or shared moments of celebration I extend my deepest gratitude. Your support has been invaluable in helping me achieve this milestone, and I am profoundly thankful for each one of you.

Prabuddhha Kant Mishra

Abstract

The field of condensed matter physics has undergone a significant transformation with the discovery of topological characteristics in materials. These nontrivial topological features, evident in electronic states and magnetic textures, hold great potential for enhancing data processing and storage capabilities, thereby accelerating advancements in quantum computation. This thesis delves into the fascinating regime of magnetic, multiferroic, and topological materials, which hold great promise for advancing spintronic devices and quantum computation. Beginning with a concise overview of fundamental concepts, the study sets the stage for a detailed exploration of how these properties interplay in various novel materials. This thesis delves into the synthesis, characterization, and physical attributes of metal chalcogenides, namely Nd_3Te_4 , Nd_3Se_4 , $\text{Ta}_2\text{Ni}_3\text{Te}_5$ and NdBiTe . These metal chalcogenides were synthesized using the solid-state sealed tube technique. In this thesis we have investigated the magnetic properties of Th_3P_4 -type materials, the topological aspects of van der Waals material $\text{Ta}_2\text{Ni}_3\text{Te}_5$, and the interplay between magnetic and topological characteristics in NdBiTe .

The intricate relationship between nontrivial magnetism and noncentrosymmetric crystal structures, mediated by the Dzyaloshinskii-Moriya interaction, has been thoroughly explored in noncentrosymmetric materials like Nd_3Se_4 and Nd_3Te_4 . Unconventional magnetism plays a pivotal role in driving advancements in spintronic applications. Through our investigation, we have meticulously probed the common attributes of competing interactions, including large magnetic irreversibility, nonsaturation of magnetization, and field-induced transitions. The study further correlates the impact of sintering conditions on magnetic and magnetocaloric properties. Notably, our observations of concomitant transitions in magnetic and specific heat investigations suggest the presence of ferromagnetic interactions and noncollinear alignment of magnetic moments, underscoring the complexity and richness of phenomena inherent in these fascinating materials.

The topological properties of $\text{Ta}_2\text{Ni}_3\text{Te}_5$ were analyzed, revealing temperature-dependent resistivity shifts from semiconducting to metallic behavior, alongside weak anti-localization signatures in magnetoresistance data. This behavior indicates the

presence of strong spin-orbit coupling and spin-momentum locking. Isothermal magnetization studies further confirmed the presence of Berry paramagnetism, underscoring the material's promising characteristics for quantum technologies. Further the interplay between magnetism and topological effects in NdBiTe, a long-range antiferromagnet. Magnetization measurements below the Néel temperature reveal spin-reorientation phenomena, supported by specific heat data indicating significant electronic correlations and crystal field splitting. The metallic transport properties of NdBiTe exhibit positive magnetoresistance over a wide temperature range, and a Kondo-like resistivity dependence below the Néel temperature suggests the presence of highly interacting fermions, corroborated by a substantial electronic specific heat coefficient.

In conclusion, this work highlights the importance of magnetic topological materials, addressing both their potential applications and the challenges in predicting and synthesizing new materials. The findings not only deepen the understanding of the interplay between magnetism and topology but also pave the way for future innovations in quantum materials and spintronic technologies.

सार

सामग्रियों में टोपोलॉजिकल विशेषताओं की खोज के साथ संघनित पदार्थ भौतिकी के क्षेत्र में एक महत्वपूर्ण परिवर्तन आया है। इलेक्ट्रॉनिक अवस्थाओं और चुंबकीय बनावट में स्पष्ट गैर-तुच्छ टोपोलॉजिकल विशेषताएं, डेटा प्रसंस्करण और भंडारण क्षमताएं को बढ़ाने की काफी संभावनाएं रखती हैं। जिससे क्वांटम गणना में प्रगति में तेजी आती है। यह थिसिस चुंबकीय, मल्टीफेरोइक और टोपोलॉजिकल सामग्रियों के आकर्षक शासन पर प्रकाश डालती है, जो स्पिट्रॉनिक उपकरणों और क्वांटम गणना को आगे बढ़ाने के लिए काफी संभावनाएं रखती है। मौलिक अवधारणाओं के संक्षिप्त अवलोकन के साथ शुरुआत करते हुए, अध्ययन इस बात की विस्तृत खोज के लिए मंच तैयार करता है कि ये गुण विभिन्न उपन्यास सामग्रियों में कैसे परस्पर क्रिया करते हैं। यह थिसिस धातु चालकोजेनाइड्स के संश्लेषण, लक्षण वर्णन और भौतिक गुणों पर प्रकाश डालती है, अर्थात् Nd_3Te_4 , Nd_3Se_4 , $Ta_2Ni_3Te_5$ और $NdBiTe$ । इन धातु चैक्लोजेनाइड्स को सॉलिड-स्टेट सीलबंद ट्यूब तकनीक का उपयोग करके संश्लेषित किया गया था। इस थिसिस में हमने Th_3P_4 -प्रकार की सामग्रियों के चुंबकीय गुणों, वैन डेर वाल्स सामग्री $Ta_2Ni_3Te_5$ के टोपोलॉजिकल पहलुओं और चुंबकीय और टोपोलॉजिकल के बीच परस्पर क्रिया की जांच की है। $NdBiTe$ में विशेषताएँ।

गैर-तुच्छ चुंबकत्व और गैर-सेंट्रोसिमेट्रिक क्रिस्टल संरचनाओं के बीच जटिल संबंध, डेज़्यालोशिंस्की - मोरिया इंटरैक्शन द्वारा मध्यस्थ, Nd_3Se_4 और Nd_3Te_4 जैसी गैर-सेंट्रोसिमेट्रिक सामग्रियों में पूरी तरह से खोजा गया है। अपरंपरागत चुंबकत्व स्पिट्रॉनिक अनुप्रयोगों में प्रगति लाने में महत्वपूर्ण भूमिका निभाता है। अपनी जांच के माध्यम से, हमने प्रतिस्पर्धा की सामान्य विशेषताओं की सावधानीपूर्वक जांच की है बड़ी चुंबकीय अपरिवर्तनीयता, चुंबकीयकरण की असंतुष्टि और क्षेत्र-प्रेरित संक्रमण सहित इंटरैक्शन। अध्ययन चुंबकीय और मैग्नेटोकलोरिक गुणों पर सिंट्रिंग स्थितियों के प्रभाव को और भी सहसंबंधित करता है। विशेष रूप से, चुंबकीय और विशिष्ट ताप जांच में सहवर्ती संक्रमणों के हमारे अवलोकन लौहचुंबकीय अंतःक्रियाओं और चुंबकीय क्षणों के गैर-कोलिनियर संरेखण की उपस्थिति का सुझाव देते हैं, जो इन आकर्षक सामग्रियों में निहित घटनाओं की जटिलता और समृद्धि को रेखांकित करते हैं।

$Ta_2Ni_3Te_5$ के टोपोलॉजिकल गुणों का विश्लेषण किया गया, जिससे मैग्नेटोरेसिस्टेंस डेटा में कमजोर एंटी-लोकलाइज़ेशन हस्ताक्षरों के साथ-साथ अर्धचालक से धातु व्यवहार में तापमान-निर्भर प्रतिरोधकता बदलाव का पता चला। यह व्यवहार मजबूत स्पिन-ऑर्बिट युग्मन और स्पिन-मोमेंटम लॉकिंग की उपस्थिति को इंगित करता है। आइसोथर्मल मैग्नेटाइज़ेशन अध्ययनों ने क्वांटम प्रौद्योगिकियों के लिए सामग्री की आशाजनक विशेषताओं को रेखांकित करते हुए, बेरी पैरामैग्नेटिज्म की उपस्थिति की पुष्टि की। इसके अलावा लंबी दूरी के प्रतिलौहचुंबक, $NdBiTe$ में चुंबकत्व और टोपोलॉजिकल प्रभावों के बीच परस्पर क्रिया नील तापमान के नीचे चुंबकीयकरण माप से स्पिन-पुनर्अभिविन्यास घटना का पता चलता है, जो विशिष्ट ताप डेटा द्वारा समर्थित है जो महत्वपूर्ण इलेक्ट्रॉनिक सहसंबंध और क्रिस्टल क्षेत्र विभाजन का संकेत देता है। एनडीबीआईटीई के धात्विक परिवहन गुण एक विस्तृत तापमान सीमा पर सकारात्मक मैग्नेटोरेसिस्टेंस प्रदर्शित करते हैं, और नील तापमान के नीचे एक कौंडो जैसी प्रतिरोधकता निर्भरता अत्यधिक इंटरैक्टिंग फर्मियन की उपस्थिति का सुझाव देती है, जो एक पर्याप्त इलेक्ट्रॉनिक विशिष्ट गर्मी गुणांक द्वारा पुष्टि की जाती है।

अंत में, यह कार्य चुंबकीय टोपोलॉजिकल सामग्रियों के महत्व पर प्रकाश डालता है, उनके संभावित अनुप्रयोगों और नई सामग्रियों की भविष्यवाणी और संश्लेषण में चुनौतियों दोनों को संबोधित करता है। निष्कर्ष न केवल चुंबकत्व और टोपोलॉजी के बीच परस्पर क्रिया की समझ को गहरा करते हैं, बल्कि क्वांटम सामग्री और स्पिंट्रॉनिक प्रौद्योगिकियों में भविष्य के नवाचारों का मार्ग भी प्रशस्त करते हैं।

Contents

Certificate	I
Acknowledgements	II
Abstract.....	V
Contents.....	IX
List of Figures.....	XIII
List of Tables.....	XXI
Abbreviations.....	XXII
Symbols.....	XXIII
1 Introduction	1
1.1 Intermetallic compounds and synthesis	1
1.2 Breaking of symmetry: Emergent properties	2
1.3 Breaking of time reversal symmetry: Magnetism	3
1.3.1 Exchange interactions	4
1.3.2 Magnetism in rare-earth element based materials	5
1.4 Band Theory of electronic states.....	6
1.5 Topology in electronic band structure	7
1.5.1 Topological Insulators	9
1.5.2 Topological semimetals.....	10
1.5.3 Dirac semimetals	12
1.5.4 Weyl semimetals	13
1.5.5 Nodal line semimetals.....	15
1.6 Research Objectives.....	16

1.7	Background and Motivation	16
1.8	Choice of materials for investigation	19
1.9	Thesis Organization	19
2	Characterization techniques	27
2.1	Synthesis	27
2.2	Characterization techniques	28
2.2.1	X-ray diffraction	28
2.2.2	Field emission scanning electron microscope	30
2.3	Property measurements	31
2.3.1	Physical Property Measurement System: PPMS	32
2.3.2	Magnetic Property Measurement System: MPMS	33
3	Competing magnetism in Th_3P_4 type of noncentrosymmetric cubic material: Nd_3Te_4	37
3.1	Introduction	37
3.2	Experimental Details	40
3.3	Outline of the Study	41
3.4	Magnetic and structural analysis for S1, S2 and S3	43
3.4.1	Structural studies	43
3.4.2	Magnetic susceptibility studies	44
3.4.3	Isothermal magnetization studies	48
3.5	Detailed investigations on S1	49
3.5.1	Magnetocaloric studies	49
3.5.2	Frequency dependent ac-susceptibility studies	53
3.5.3	Transport and Magnetotransport studies	56
3.5.4	Specific heat studies	57
3.6	Experimental investigations and results for S3	60
3.6.1	DC Magnetization studies	60
3.6.2	Isothermal Magnetization studies	63
3.6.3	Magneto-entropic studies	67
3.6.4	AC-susceptibility studies	69
3.7	Discussion	72
3.8	Conclusions	75
4	Multiple magnetic phases and nontrivial behaviour in noncentrosymmetric cubic lattice: Nd_3Se_4	77
4.1	Introduction	77
4.2	Experimental Details	79
4.3	Experimental investigations and results	81
4.3.1	Structural studies	81
4.3.2	dc Magnetization studies	82

4.3.3	Isothermal Magnetization studies	85
4.3.4	Magnetocaloric studies	88
4.3.5	ac-susceptibility studies	90
4.3.6	Specific Heat studies	96
4.3.7	Transport and Magnetotransport studies	98
4.4	Discussion	101
4.5	Conclusions	103
5	Weak anti-localization and spin-momentum locking in topological insulator $\text{Ta}_2\text{Ni}_3\text{Te}_5$	105
5.1	Introduction	105
5.2	Experimental Details	108
5.3	structural studies	109
5.4	Transport Properties	109
5.5	perpendicular magnetotransport	117
5.6	Magnetic properties	120
5.7	Specific heat	123
5.8	Conclusions	125
6	ZrSiS type square-net antiferromagnetic nonsymmorphic semimetal: NdBiTe	127
6.1	Introduction	127
6.2	Experimental and Computational Details	130
6.3	Results and Discussion	133
6.3.1	Temperature Dependent Magnetic Susceptibility	134
6.3.2	Isothermal Magnetization	135
6.3.3	Specific Heat	138
6.3.4	Transport and Magnetotransport Properties	140
6.3.5	First-Principles Calculations	142
6.4	Conclusions	149
7	Future prospects	151
7.1	Conclusions	151
7.2	Future prospects	154
7.2.1	Higher-Order Topology	155
7.2.2	Creating Exotic Magnetic Textures:	156
7.2.3	Fine-Tuning Magnetism:	156
7.2.4	Search for new candidate materials	157

Bibliography

159

List of Figures

1.1	(a) Realization of Various electronic topological phases (reproduced from Annu. Rev. Condens. Matter Phys. 8:337-354)	11
1.2	(a) The weyl nodes connected with Fermi arc.(b) The existence of chiral anomaly for applied magnetic and electric field in the same direction. (reproduced from Annu. Rev. Condens. Matter Phys. 8:337-354)	14
2.1	(a)Diffraction of X-rays from a set of atomic planes under Bragg’s condition of inelastic interaction. (b) Schematic of a x-ray diffractometer operating in Bragg-Brentano geometry.	29
2.2	(a) Schematic representation of the electron beam in SEM (b) The experimental set-up of SEM (Zeiss EVO 50).	30
2.3	(a) Diagram for the internal instrumentation of PPMS (b) various parts of electrical measurement probe (for CFMS-PPMS Cryogenics Ltd).	33
2.4	Simplified schematic diagram of a SQUID magnetometer with 2nd order gradiometer. The inset shows the SQUID response versus sample position (reproduced from J. Appl. Phys. 124, 161101 (2018)) (b) Superconductor Ring that has two isolating connectors.	34
3.1	(a) Rietveld refinement of room temperature powder X-ray diffraction data of polycrystalline Nd_3Te_4 . Vertical bars indicate the allowed Bragg’s reflections for Nd_3Te_4 . The blue line indicates the difference between the observed and the fitted patterns. (b) The unit cell of Nd_3Te_4 with 4 formula units (c) Structure viewed from the 3-fold rotational axis (d) The polyhedra of Nd ion surrounded by 8 Te, and Te surrounded by 6 Nd.	39
3.2	The EDAX pattern of all three samples sintered at different temperatures verifying the elemental ratio.	42

3.3	(a) Temperature-dependent magnetic susceptibility $\chi(T)$ data under ZFC and FC protocol at $H = 500$ Oe, inset shows the first-order derivative of ZFC data as a function of temperature, the solid brown curve is guide to the eye. The T_C is marked by the dashed blue line. (b) The ac-susceptibility data as a function of temperature from 2 K to 40 K, shows both in-phase (χ') and out-of-phase (χ'') components for $H_{ac} = 3$ Oe and $f = 33$ Hz. (c) ZFC $\chi(T)$ data under $H = 10$ kOe in the temperature range of 2 K to 300 K, corresponding the $\chi^{-1}(T)$ data fit with modified CW equation shown by blue solid line.	46
3.4	(a) Isothermal magnetization $M(H)$ data at 2 K, in the field range of ± 70 kOe for all three samples as marked. (b) The virgin $M(H)$ curves at different temperatures across the transition temperature (c) corresponding Arrott plots at temperatures ranging from 2 K to 54 K with an interval of 2 K. (d-e) The change in entropy (ΔS_M) as a function of temperature for various applied field range, details discussed in the text.	47
3.5	(a) and (b) show in-phase and out-of-phase components of AC-susceptibility data, respectively, as a function of temperature for various applied frequencies (3 Hz to 673 Hz). The inset of (a) shows the shift in the peak position with an increase in the frequency in the expanded temperature scale. (c) Power law fit to show variation in T_f with change in applied frequency. (d) The Vogel-Fulcher fit, details are described in the text part.	52
3.6	(a) The temperature dependent resistivity $\rho(T)$ in the range of 2-300 K at $H = 0$ kOe, inset shows the logarithmic dependence of resistivity (b) $\rho(T)/\rho(100)$ at various applied field. (c) Isothermal MR at various temperatures across magnetic transition temperature in the field range of ± 70 kOe.	56
3.7	(a) specific heat as a function of temperature in the range of 2-200 K for $H = 0$ T, the Debye fit is shown by the red solid line. The inset shows the expanded scale view for the low-temperature regime (b) C/T vs T having a peak centered at 46 K corresponding to the Schottky anomaly. The inset shows C/T vs T^2 for $H = 0$ and 5 T and is explained in the text.	58
3.8	The magnetic susceptibility ($\chi(T)$) as a function of temperature in zero-field-cooling (ZFC) and field-cooling (FC) at an applied field of (a) 1 kOe (logarithmic temperature scale) and (c) 30 kOe, inset shows the corresponding inverse susceptibility plots as a function of temperature for the applied field of (a) 1 kOe and (b) 30 kOe, fitted with the modified C-W model equation 2, shown by a red solid line in high-temperature regime. (c) shows the suppression of bifurcation between ZFC and FC with an increase in the applied field and derivatives of FC data with respect to temperature are shown in (d), the inset of (d) shows the variation of T_C with an increase in H	61

3.9	<p>(a) The isothermal magnetization $M(H)$ data as a function of the applied field in the range ± 7 T, at different temperatures across T_C. (b) The variation in the coercive field with an increase in the temperature. The red solid line shows a linear dependence of logarithmic at low temperatures and deviation at higher temperatures. (c) The Virgin isothermal ($M(H)$) data plotted as a function of field at $T = 2$ K and derivative of the same (dM/dH), which signifies field-induced phase transition at $H = 4.25$ kOe as indicated by the vertical solid blue line. The lower panel of (c) shows derivative plots for various temperatures from 2 K to 20 K with an interval of 2 K. (d) Arrott plots corresponding to $M(H)$ virgin plots, the one corresponding to T_C is indicated by a linear fit. (e) The Arrott plot at $T = 2$ K in log-log scale for a clear representation of sign change in the slope.</p>	65
3.10	<p>The change in magnetic entropy (ΔS_M) as a function of temperature for various applied field intervals. The insets of each figure show the derivative of magnetization for data measured at the particular field (in ZFC mode), the field of $M(T)$ lies in the field regime of the corresponding figure. The field range varies as (a) $2 \text{ Oe} < H < 30 \text{ Oe}$, (b) $30 \text{ Oe} < H < 1 \text{ kOe}$, (c) $1 \text{ kOe} < H < 10 \text{ kOe}$, and (d) $10 \text{ kOe} < H < 70 \text{ kOe}$.</p>	66
3.11	<p>ac-$\chi(H)$ data in the temperature range 30-42 K for applied field $H_{ac} = 3$ Oe at different excitation frequency for the different applied dc-magnetic fields (a) in-phase and (b) out-of-phase component. The arrow indicates the shift of the peak position, which is shown as a function of the applied field in the inset. The normalized (c) in-phase and (d) out-of-phase isothermal ac-$\chi(H)$ data as function of H in the range of 0-1 kOe at various temperatures across the T_C. Zoomed-in view at low applied field range (0-100 Oe) for the normalized (e) in-phase and (f) out-of-phase isothermal ac-$\chi(H)$ data.</p>	70
3.12	<p>The in-phase ac-$\chi(H)$ data in the field range of 0-80 Oe at various applied excitation frequencies for different temperatures. The corresponding insets for each figure show the dc-$M(H)$ data (black) and its derivative (dM/dH) as function of the applied field. The constant temperatures are (a) 37 K, (b) 39 K, and (c) 41 K.</p>	71

3.13	(a) The temperature-dependent magnetization ($M(T)$) data taken ZFC and FC mode for low applied field ranging from 3 Oe to 26 Oe. The obtained magnetization value for FC mode at $T = 20$ K. (b) The derivatives as a function of temperature for different applied fields for both FC (upper panel) and ZFC (lower panel) modes. The arrow indicates the increasing field. The derivatives as a function of temperature for both FC and ZFC modes at $H = 3$ (left panel) and 24 Oe (right panel). (d) The ($M(T)$) data under FCC and FCW protocols of measurements (indicated by curved arrows) for different applied fields. The associated thermal hysteresis is shown in the zoomed scale for $H = 10$ and 100 Oe.	72
4.1	(a) Rietveld refinement of room temperature powder X-ray diffraction data of polycrystalline Nd_3Se_4 . Vertical lines indicate Bragg's reflections for the material. The blue line indicates the difference between the observed and the simulated patterns. (b) The unit cell of Nd_3Se_4 with 4 formula units (c) Structure viewed from the body-diagonal having 3-fold rotational axis (d) The attached polyhedra of Nd ion surrounded by 8 Se, and Se coordinated with 6 Nd.	79
4.2	The magnetic susceptibility ($\chi(T)$) as a function of temperature in zero-field-cooling (ZFC) and field-cooling (FC) at an applied field of 1 kOe (upper panel) and 30 kOe (lower panel), inset shows the corresponding inverse susceptibility plots as a function of temperature, fitted with the modified C-W model equation 2, shown by a blue solid line in high-temperature regime. (b) shows the suppression of bifurcation between ZFC and FC with an increase in the applied field (c) the derivatives of ZFC (upper panel) and FC (lower panel) data with respect to temperature, the inset of upper panel shows the variation of T_{irr} with an increase in H , fit with Almeida-Thouless line. (d) Shift in the T_C with the applied field.	81
4.3	(a) The isothermal magnetization $M(H)$ measurements as a function of the applied field ± 7 T, at different temperatures across T_C (b) The logarithmic variation of H_C with applied temperature (below 40 K). (c) In the upper panel, the virgin curve and corresponding derivative with respect to field dM/dH at 2 K and the peak indicated by the blue solid line. The dotted circle shows the to get attention at complex phases low field regime ($H < 1\text{kOe}$). The lower panel shows the same derivative plots as the upper one at various temperatures in the range of 2-30 K. (d) Arrott plots corresponding to $M(H)$ virgin plots, infer T_C , indicated by the black solid line. (e) Arrott plots at $T = 2$ K, to emphasize the field-induced transition from negative to positive slope at circle field.	83

4.4	Magnetization entropy as a function of temperature ranging from 4 to 65 K in the different applied field regimes, with the solid line indicating the direction of the increasing field. The insets show the derivation of ZFC magnetization data at particular H and belong to the field regime of the corresponding figure. (a) In the low field range from 100 Oe to 1 kOe, the inset shows the derivation of ZFC magnetization data at $H = 1$ kOe. (b) In the intermediate field range from 1 to 10 kOe, the inset shows the derivation of ZFC magnetization data at $H = 1$ kOe. (c) In the high field regime, from 10 to 70 kOe, the inset shows the derivation of ZFC magnetization data at $H = 30$ kOe.	88
4.5	The (a) real and (b) imaginary components of ac-susceptibility data for applied field $H_{ac} = 3$ Oe at various excitation frequencies. The arrow indicates the shift in peak towards to higher temperature with an increase in frequency. (c) The power law fit and (d) the Vogel-Fulcher fit to obtain relevant parameters, details discussed in the text.	91
4.6	(a) Real and (b) imaginary parts of ac-susceptibility data at an excitation frequency of 31 Hz in the temperature range 40-56 K for various applied fields from $H_{ac} = 0$ Oe to 1 kOe. The inset shows the variation of peak positions for both components as a function of the field. (c) Real and (d) imaginary parts of field dependent $\chi'(H)$ data in the H range of ± 2 kOe at various temperatures. The inset shows the same data in the logarithmic scale to highlight the slope change. (e) Real and (f) imaginary parts of the field-dependent $\chi'(H)$ data, normalized with respect to χ'_0 , for applied field range of 0-80 Oe, at various temperatures.	93
4.7	(a) in-phase ac-susceptibility data (blue) and dM/dH of dc-magnetization as function of applied field at $T = 53$ K, both having a kink in the low field regime for the applied field. The inset shows the data points of $M(H)$ at 53 K, indicated for spontaneous magnetization.	94
4.8	(a) The specific heat data $C(T, H = 0)$ as a function of temperature, having peak at T_C with ΔC of 29.43 J/K f.u. (b) The C/T vs. T^2 plot, linear fit with the $\gamma + \beta T^2$, depicted by red solid line. (c) $C(T, H)$ data under various applied magnetic field.	95
4.9	(a) The temperature dependence of resistivity data $\rho(T, H = 0)$ in the temperature range of 2-300 K, linear fit in the temperature of $T_C < T < 300$ K, shown by green solid line. The inset shows the quadratic temperature dependence of ρ and fit with $\rho_0 + AT^2$ in the temperature range of $10 \text{ K} < T < T_C$ indicated by the blue solid line. (b) $\rho(T)$ data in the temperature range of 2-120 K under various applied magnetic fields (upper panel). The lower panel shows the corresponding MR plots. (c) The symmetrical magnetoresistance at $T = 2$ K in the field range of ± 7 T, the critical field shown by black dotted lines.	98

5.1	(a) Rietveld refinement of room temperature powder XRD data of polycrystalline bulk $\text{Ta}_2\text{Ni}_3\text{Te}_5$. Vertical bars represent the 2θ positions for allowed Bragg's reflections of $\text{Ta}_2\text{Ni}_3\text{Te}_5$. The blue line is the difference between the observed and the fitted patterns. (b) Stacked layers of material, visible in SEM image of the sample, along with elemental mapping (c) Crystal structure of $\text{Ta}_2\text{Ni}_3\text{Te}_5$, layers stacked along a-axis. Various metal-centered polyhedron and metal-cluster of Ta_2Ni_2 are depicted on both sides of the unit cell.	110
5.2	(a) Resistivity as a function of temperature (logarithmic scale) showing semiconducting to semimetallic transition for polycrystalline $\text{Ta}_2\text{Ni}_3\text{Te}_5$ at around 7 K, indicated by a dotted line. (b) Arrhenius fit for high-temperature data (180-300 K), shown by solid red line. (c) Electrical conductivity as a function of $T^{-1/4}$. The VRH fit for conductivity is shown in the solid red line, having deviation from data at low temperature. (d) The resistivity, normalized w.r.t. resistivity at 300 K ($\rho(300)$), as a function of temperature at various applied magnetic field perpendicular to the current direction.	113
5.3	(a)MR(%) as a function of applied magnetic field up to 14 T at 2 K, a linear fit is shown at higher field range (from 5 T to 14 T) by the red line, inset shows MR(%) as a function of applied magnetic field (± 5 T) perpendicular and parallel to the current direction at 2 K. (b) MR(%) at various temperatures from 2K to 7K with $\Delta T = 1$ K, in range of applied field from -5T to 5T perpendicular to current direction. (c) MR(%) at various temperatures from 2K to 7K with $\Delta T = 1$ K, in the applied field (± 5 T) parallel to the current direction. (d) Kohler's plot corresponding to magnetic field perpendicular to the current direction.	116
5.4	(a) Magnetoconductance as a function of the applied field, fitting curves for simple and Modified-HLN equations. Modified-HLN equation is providing a better fit of data (b) Magnetoconductance fitted with modified-HLN equation at different temperatures from 2 K to 7 K with $\Delta T = 1$ K. (c) Variation of normalized α with temperature. (d) Variation of B_ϕ and l_ϕ with temperature.	119
5.5	(a) Magnetic susceptibility of $\text{Ta}_2\text{Ni}_3\text{Te}_5$ in Zero field cooled and field cooled protocol as a function of temperature for the applied field of 2 T. (b) Isothermal magnetization at 2, 5 and 300 K. (c) Magnetic susceptibility (M/B) as a function of the applied magnetic field at different temperatures, cusp at the low applied field is clearly visible. (d) The schematic E-K diagram of Dirac-like electronic state, enriched in topological materials	123
5.6	(a) Specific heat of $\text{Ta}_2\text{Ni}_3\text{Te}_5$ as a function of temperature at zero magnetic field, inset shows expanded view of C vs. T data in low-temperature regime (b) C/T vs. T^2 plot in low-temperature regime ($T \leq 10$ K); fit with $C/T = \gamma + \beta T^2$ is shown by the red solid line.	124

6.1	(a) Rietveld refinement of room temperature powder X-ray diffraction data of polycrystalline NdBiTe. Vertical bars show the allowed Bragg's peak for NdBiTe. The blue line represents the difference in the experimental and simulated patterns. (b) Shows the Crystal structure of NdBiTe, with constituents of polyhedra around Nd ion and the square-net layer of Bismuth, mentioned with various interatomic distances in Å unit. (c) The SEM image shows the layered nature of the specimen along with elemental mapping to show the homogeneous distribution of elements.	131
6.2	(a) Magnetic susceptibility ($\chi(T)$) and corresponding inverse susceptibility ($\chi^{-1}(T)$) in zero-field-cooling (ZFC) and field-cooling (FC) at different fields (1, 10 and 50 kOe). $\chi^{-1}(T)$ at the applied field of 50 kOe, fitted with modified C-W model, shown by red solid line. (b) Variation of ZFC $\chi(T)$ at various applied magnetic fields in low-temperature regime (2-25 K), the inset shows the suppression of T_N as a function of the applied field. (c) The χ' and χ'' components of ac-susceptibility data in the temperature range of 2-15 K at 3 and 91 Hz frequencies.	132
6.3	(a) Isothermal magnetization (MH) data as a function of applied magnetic field at 2 and 5 K. (b) dM/dH as a function of applied magnetic field at various temperatures across the magnetic transition from 2 K to 8 K, with $\Delta T = 1$ K. The dotted red lines show the critical fields (H_{C1} and H_{C2}) for 2 K curve, as a case of representation. (c) The corresponding Arrott plots and inset demonstrates the change in entropy of magnetization as a function of temperature for various fields ranging from 10 kOe to 70 kOe.	134
6.4	(a) The specific heat data as a function of temperature in the absence of applied magnetic field. The inset shows C/T vs. T^2 plot fit (solid red line) with equation $\gamma + \beta T^2$. (b) C/T vs. T plot signifying the peak centered at 48 K, corresponding to Schottky anomaly. The inset shows a temperature-dependent specific heat at various applied magnetic fields.	136
6.5	(a) Temperature-dependent resistivity $\rho(T)$ in 2 - 300 K range. The solid red line shows a fit to BG equation in the high-temperature regime. The inset shows $\rho(T)$ data in logarithmic scale, where the dotted red lines represent an upturn in $\rho(T)$ at ≈ 16 K and a slope change at T_N . (b) The MR data as a function of H at different temperatures. (c) The smoothed MR data as function of H and its first derivative with respect to the applied field. The dotted lines indicate the critical fields.	138

6.6	The density of states and atom-projected density of states (a) without and (b) with spin-orbit coupling. Insets in panels (a) and (b) represent the orbital resolved density of states. The electronic band structure of NdBiTe (c) GGA+U (d) GGA+U+SOC. The Fermi level is set to zero.	144
6.7	The schematic of (a) FM, (b) AFM-A and (c) AFM-I magnetic configurations. The panel (d) represents the octahedral filling of electrons in f -state of Nd ion.	146
6.8	The enlarged view of electronic structure of NdBiTe at high symmetry point R for (a) without SOC and magnetism, (b) without SOC and with magnetism, (c) with SOC and without magnetism, and (b) with SOC and magnetism.	147
6.9	The calculated (a) phonon dispersion (b) phonon density of states and (c) Temperature dependence of specific heat at constant volume for NdBiTe.	147

List of Tables

3.1	Wyckoff positions, atomic coordinates, occupancy and isothermal parameters of atoms for all three samples of Nd_3Te_4	42
3.2	Magnetic parameters for the three samples, extracted from $\chi(T)$ at 10 kOe and $M(H)$ at 2 K, with their respective units.	44
3.3	The magnetic transition temperature and maximum entropy change $-\Delta S_M$ for ΔH - 0-5 T.	52
3.4	Magnetic parameters of Nd_3Te_4 , with their respective units.	62
4.1	Structural, magnetic, thermal and transport parameters of Nd_3Se_4 , with their respective units.	80
5.1	Refined structural parameters of $\text{Ta}_2\text{Ni}_3\text{Te}_5$ in their respective units.	111
6.1	Structural and magnetic parameters of NdBiTe in their respective units.	131
6.2	Calculated total energy (in meV) of FM and AFM-A configurations relative to that of AFM-I configuration, and the magnetic moments (in μ_B) of the constituent atoms.	143

Abbreviations

ARPES	A ngle R esolved P hoto E mission S pectroscopy
TI	T opological I nsulator
TSM	T opological S emimetal
DSM	D irac S emimetal
WSM	W eyl S emimetal
NLSM	N odal L ine S emimetal
BZ	B rillouin Z one S emimetal
IS	I nversion S ymmetry
NCS	N on C entro S ymmetric
TRIM	T ime R eversal I nvariant M omenta
RKKY	R uderman K ittel K asuya Y osida
DMI	D zyaloshinskii M oriya I nteraction
SEI	S ymmetric E xchange I nteraction
DMS	D iluted M agnetic S emiconductor
SOC	S pin O rbital C oupling
XRD	X R ay D iffraction
SEM	S canning E lectron M icroscopy
SQUID	S uperconducting Q uantum I nterference D evice
PPMS	P hysical P roperty M easurement S ystem
EDX	E nergy D ispersive X ray analysis
WAL	W eak A nti L ocalization
FM	F erro M agnetic
AFM	A nti F erro M agnetic
DFT	D ensity F unctional T heory

Symbols

c	speed of light in vacuum
ϵ	dielectric constant/permittivity
k_0	wavevector in free space
μ_{eff}	effective magnetic moment
M	Magnetization
ω	angular frequency
λ	wavelength
n_r	reference refractive index
\hbar	reduced Planck's constant
l	orbital angular momentum in units of $2\pi\hbar$